Research Article | Vol. 8, No. 12 | 1 Dec 2018 | OPTICAL MATERIALS EXPRESS 3787
Optical Materials EXPRESS

Plasmon-enhanced upconversion: engineering enhancement and quenching at nano and macro scales

ILIA L. RASSKAZOV,[1] LANG WANG,[1,2] CATHERINE J. MURPHY,[3] ROHIT BHARGAVA,[2,3,4] AND P. SCOTT CARNEY[1,*]

[1]*The Institute of Optics, University of Rochester, Rochester, NY 14627, USA*
[2]*Department of Electrical & Computer Engineering, University of Illinois at Urbana-Champaign, Urbana, IL 61801, USA*
[3]*Department of Chemistry, University of Illinois at Urbana-Champaign, Urbana, IL 61801, USA*
[4]*Beckman Institute for Advanced Science and Technology, Departments of Bioengineering, Chemical and Biomolecular Engineering, and Mechanical Science and Engineering, University of Illinois at Urbana-Champaign, Urbana, IL 61801, USA*
[*]*scott.carney@rochester.edu*

Abstract: Photon upconversion (UC) is the sequential absorption of two or more low frequency photons and subsequent emission of light at a higher frequency. Because of a large number of potential applications of this anti-Stokes process, extensive studies of UC have taken place in the last decades. The most crucial challenge in this field is the development of an efficient strategy to enhance the inherently low efficacy of the UC process. Among the various intensively developed approaches, local tailoring of the electromagnetic field with metal nanoparticles (MNPs) to the position of the UC material has been considered as the most promising one. However, distinctive features of photon UC imply the emergence of fluorescence quenching near the MNP. Along with different near-and far-field MNP responses and non-trivial competition of enhancement and quenching of the UC signal in suspension of MNPs on the macroscale, the search of optimal MNP configuration for UC enhancement becomes quite the challenging task to solve. In this paper, we thoroughly analyze these effects with a rigorous and comprehensive theoretical model based on the extended Mie theory for multilayered spheres and the effective medium approach. We provide general guidelines for highly efficient UC enhancement by Ag and Au spherical MNPs.

1. Introduction

The absorption of low-energy photons and their re-emission at higher frequencies through the upconversion (UC) process has attracted significant attention for a long time [1] due to the endless number of potential applications [2] with particular interest in biology [3–7], imaging [8], solar energy harvesting [9–12], and nanoscopy [13, 14]. However, strictly limited wide-spread practical implementation of inherently low-efficacy UC process has stimulated the emergence of various strategies for its enhancement in a last decade [15]. These strategies include broadband absorption [16], triplet-triplet annihilation [17, 18], high excitation irradiance [19], enrichment of molecular antenna triplets [20], phonon mediated enhancement [21]. Apart from these strategies, nanoscale tailoring of the electromagnetic field to the position of the UC material via metal nanoparticles (MNPs) has been considered as the most promising way to enhance UC process [22–24]. Termed plasmon-enhanced UC, such straightforward yet non-trivial approach is enabled by the unique property of MNPs to support collective electron oscillations – localized surface plasmon resonances (LSPRs) [25]. These optical excitations can be confined well below the diffraction limit of light with high degree of the local electric field enhancement, which paves a way for efficient UC enhancement. While numerous works in the field of plasmon-enhanced UC

#345738 https://doi.org/10.1364/OME.8.003787
Journal © 2018 Received 12 Sep 2018; revised 18 Oct 2018; accepted 18 Oct 2018; published 9 Nov 2018

Optical Materials EXPRESS

report quite promising UC enhancement factors (up to several thousands [26]), there is a crucial lack of fundamental studies of this process both in terms of *local* near-field interactions between UC material and MNP, and *macroscale* UC enhancement in a suspension of plasmonically enhanced UC material. As a result, most of theoretical and experimental studies usually disregard a number of important features, and report only the possibility to enhance UC with MNP without further optimization which may yield in considerably higher UC enhancement factors.

First important feature is related to strong fluorescence quenching [27] near the metal surface due to the presence of a real intermediate state, which is populated before the final emitting state during the UC process. This leads to a competition between high local field enhancement and strong fluorescence quenching near the MNP, which is usually controlled by a dielectric spacer layer introduced between MNP and UC material [28, 29] to suppress quenching. However, the pattern of the local field distribution [30] and fluorescence of the dipole emitter [31] near the dielectric-covered MNP is completely different compared with bare MNP. Nonetheless, the necessity of simultaneous estimating of both electric field enhancement and decay rates using time-consuming full-field simulations usually implies the ignoring of dielectric spacer presence [32] due to high complexity of calculations.

Next, the presence of the spectral shift between near and far-field MNP response [33] is usually underestimated [34–38], and 'optimal' MNP is chosen by tailoring its LSPR to excitation or emission frequency of the UC process. However, the interaction between the UC material and the MNP takes place in a near-field, while commonly utilized extinction cross-section is a quantity measured in the far-field. Taking into account large spectral shift between UC excitation and emission frequencies, the importance of off-resonance plasmon-enhanced UC is usually overlooked.

Finally, *local* UC enhancement in a single UC particle attached to MNP, might be not the appropriate parameter which has to be chosen to characterize the UC enhancement in MNPs suspensions or arrays [39–46]. It was recently shown, that the competition between the enhancement and extinction of pump and signal propagating through the slab of MNPs on a *macroscopic* scale requires the development of more sophisticated theoretical approach to predict the actual recorded signal, for example, in surface-enhanced Raman spectroscopy (SERS) [47, 48] or in surface-enhanced femtosecond stimulated Raman spectroscopy (SE-FSRS) [49, 50]. Although the UC process differs [22] from SERS and SE-FSRS, one could expect the emergence of similar competition effects in the suspension of plasmonically enhanced UC particles.

Therefore, balancing between the enhancement and suppression of the UC process by a single MNP at *nano* scale, distinguishing *near*- and *far*-field response of MNPs, and competition between enhancement and extinction of both pump and upconverted signals in solution of plasmonically enhanced UC particles at *macro* scale are of particular interest for the field of plasmon-enhanced UC. In this paper, we derive the self-consistent theory to describe these phenomena. Taking into account uncountable possibilities for plasmon-enhanced strategies due to large variety of plasmonic materials and geometries of MNPs, we limit the discussion with spherical MNPs and classic plasmonic materials: Au and Ag. Rigorous Mie theory extended to multilayered spherical MNPs has been used to get the classic dipole decay rate of the emitter and local field enhancement in the vicinity of the multilayered MNP, while effective medium approach has been used to describe enhancement and extinction phenomena in a slab of MNPs with attached UC particles.

2. Theory

2.1. UC enhancement by a single MNP

The UC is a two-step process which is represented by (i) excitation (absorption) at frequency ω_{ex} and (ii) emission at frequency ω_{em}. The simplified diagram of transitions in the commonly

Optical Materials EXPRESS

used UC crystal [51,52] is depicted in Fig. 1(a). Either of these processes can be enhanced by electromagnetic field localized near a MNP, depending on the LSPR frequency ω_{LSPR} of MNP. Though various shapes of MNPs for UC enhancement have been proposed so far [26,32,53], we limit our discussion to MNPs with spherical shape.

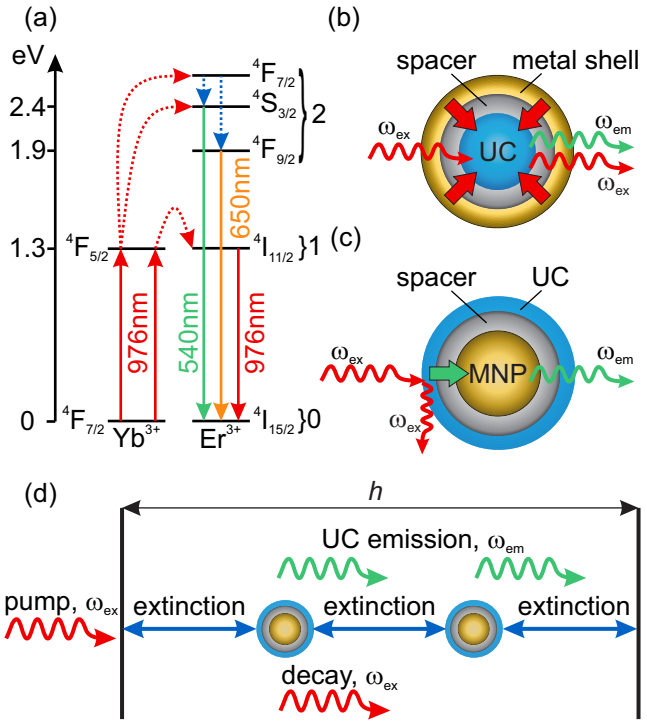

Fig. 1. Plasmon-enhanced UC process. (a) Simplified energy diagram for energy-transfer UC between Yb^{3+} and Er^{3+}. Solid arrows denote absorption and emission, dotted red arrows denote interspecies energy transfer, and dotted blue arrows denote nonradiative relaxation; (b) Excitation enhancement of UC process for UC material embedded in the metal shell; (c) Emission enhancement of UC process for UC material attached to MNP. Dielectric spacer layer introduced in both cases to suppress quenching of UC; (d) Schematic representation of signal propagation through the slab of plasmonically enhanced UC material.

Commonly, UC materials absorb light at near-IR wavelengths, thus, the utilization of *homogeneous* spherical MNPs with LSPR frequency ω_{LSPR} lying within the visible wavelength range (which is common property of classic plasmonic Ag and Au homogeneous MNPs) does not have prospects in this case. However, LSPR peak of *multilayered* spherical nanoparticles with dielectric core and metal shell, lies within the near-IR range. MNPs with this configuration are widely used in biomedicine [54] due to the ability to tailor ω_{LSPR} to biological transparency window. It should be noticed, however, that the UC process implies the presence of additional intermediate spacer layer between the UC material and metal shell, thus, the most suitable geometry for spherical multilayered particle for enhancing the UC *excitation* is: UC core / dielectric spacer / metal shell [55–58], as shown in Fig. 1(b).

Let us assume that the UC material is illuminated by the incident field $\mathbf{E}$ at frequency ω_{ex} which corresponds to transition from state $|0\rangle$ to state $|1\rangle$. According to Fermi's golden rule, the corresponding transition rate γ_{01} of electrons is then described as:

Optical Materials EXPRESS

$$\gamma_{01} = \frac{2\pi}{\hbar} |\langle 1|\mathbf{E}\cdot\mathbf{p}|0\rangle|^2 \rho_1, \tag{1}$$

where $\hbar$ is the reduced Planck's constant, $\mathbf{p}$ is the transition dipole moment, and ρ_1 is the density of final states. The emission of the upconverted signal occurs after the absorption of two photons with transition from ground state $|0\rangle$ to state $|2\rangle$ through real intermediate state $|1\rangle$. Thus, the gain to the intensity I of the emitted light through such an excitation is proportional to $|\mathbf{E}|^4$.

Multilayered MNPs are recognized as a powerful tool for manipulation and enhancement of local electric field [59,60] up to $|\mathbf{E}'|^4/|\mathbf{E}|^4 \approx 10^{10}$ or even higher, where $\mathbf{E}'$ is a local electric field in the presence of a MNP. However, the real intermediate state $|1\rangle$ which should be proceeded before populating the final emitting state $|2\rangle$ implies the existence of decay pathways from state $|1\rangle$, which have to be taken into account when calculating the overall UC enhancement. MNP can also significantly alter corresponding total decay rate γ_{tot} from the state $|1\rangle$ due to quenching of fluorescence [27]. Combining these two competing factors (simultaneous enhancement of local field and total decay rate), the overall excitation enhancement can be found as [34]:

$$f_{\text{ex}} = \frac{|\mathbf{E}'\cdot\mathbf{p}|^4}{|\mathbf{E}\cdot\mathbf{p}|^4}\frac{\gamma_{\text{tot}}}{\gamma'_{\text{tot}}}, \tag{2}$$

where prime denotes the values modified in the presence of a MNP. Both local field $\mathbf{E}'$ and γ'_{tot} rapidly increase near the surface of MNP, which results in non-trivial competition between these two factors and gives rise to complicated behavior of the overall enhancement factor f_{ex} [32].

The local field enhancement $|\mathbf{E}'|^4/|\mathbf{E}|^4$ in the vicinity of homogeneous or multilayered MNP can be found within the framework of rigorous Mie theory via well-established procedures [59,60]. Though, the calculation of $\gamma'_{\text{tot}}/\gamma_{\text{tot}}$ for dipole emitter located inside the multilayered sphere is a complicated task which is usually solved with time-consuming full field simulations. However, in this work we use purely theoretical self-consistent solution based on rigorous Mie theory [61], which is usually overlooked in the literature. Corresponding equations for $|\mathbf{E}'|^4/|\mathbf{E}|^4$ and $\gamma'_{\text{tot}}/\gamma_{\text{tot}}$ are given in the Appendix.

It should be noticed, that in principle, the maximum reachable local UC excitation enhancement is only limited with the appropriate choice of MNP geometry which provides desirable interplay of the local field enhancement and fluorescence quenching. In this case, suppressed quenching in plasmonic nanocavities [62] and nanogaps [63], enhanced emission of visible light in nanomatryoshkas [64] or tailoring the electric field away from metal surface in regular $2D$ arrays of MNPs embedded in multilayered environment [65] may play a crucial role for reaching high values of f_{ex}.

UC materials emit light at frequencies within the visible range, which makes homogeneous spherical MNPs perfect candidates for enhancing this process. Taking into account fluorescence quenching, the optimal geometry for enhancing UC *emission* is: MNP / dielectric spacer / UC material, as shown in Fig. 1(c).

Let us assume that UC particle in free space can be described as a dipole emitter with initial quantum yield $\eta_0 = \gamma^0_{\text{rad}}/\left(\gamma^0_{\text{rad}} + \gamma^0_{\text{nrad}}\right)$, where γ^0_{rad} and γ^0_{nrad} are radiative and nonradiative decay rates, correspondingly. In the presence of a MNP, this quantum yield is modified to $\eta' = \gamma'_{\text{rad}}/\left(\gamma'_{\text{rad}} + \gamma'_{\text{nrad}}\right)$. Thus, the emission enhancement can be explicitly defined as:

$$f_{\text{em}} = \frac{\eta'}{\eta_0}. \tag{3}$$

Classical theory for dipole decay rates of molecules in the presence of a spherical MNP assumes that intrinsic losses are absent in the dipole emitter [66], i.e. $\gamma^0_{\text{nrad}} = 0$. However, for UC material this is not the case: dotted blue lines in Fig. 1(a) denote nonradiative relaxation. Therefore, it is

Optical Materials EXPRESS

convenient to rewrite Eq. (3) in terms of the Purcell factor $F = \gamma'_{\text{rad}}/\gamma^0_{\text{rad}}$ and so-called antenna efficiency [32] $\eta_a = \gamma'_{\text{rad}}/\gamma'_{\text{tot}}$, where γ'_{tot} is the plasmon-modified total decay rate for a dipole emitter *without* intrinsic losses. Thus, Eq. (3) can be written as follows [67]:

$$f_{\text{em}} = \frac{1}{(1-\eta_0)/F + \eta_0/\eta_a}. \tag{4}$$

It can be seen that classical theory for dipole emitter decay rates without intrinsic losses can be applied for estimation of f_{em} by setting up appropriate values of η_0 for each particular case of UC material. Expressions for γ'_{rad} and γ'_{tot} are given in the Appendix.

It is worth to mention here, that quantum yield of the dipole emitter has a maximum value of 0.5 for a two-photon process. Therefore, unlike excitation enhancement, the values of emission enhancement are strictly limited to $f_{\text{em}} \leq 0.5/\eta_0$. In this case, one should be careful when comparing f_{em} for various scenarios, because what really matters here is the plasmon-enhanced quantum yield η' of the UC material.

2.2. Extinction in a slab of MNPs

Let us now consider light propagation in a slab of MNPs with attached UC particles embedded in a non-absorbing medium with real refractive index m_b. In this case, both pump and *locally* enhanced upconverted signals intensities I decay during propagation through the slab in accordance with the Beer's law:

$$I(h) = I(0)\exp(-\alpha h), \tag{5}$$

where h is the propagation distance, and $\alpha = 2k\text{Im}\tilde{m}$ is the absorption coefficient in a medium with complex refractive index $\tilde{m}$ [68]:

$$\tilde{m} = m_b\left[1 + i\frac{2\pi\rho}{k^3}S(0)\right], \tag{6}$$

where k is the wave vector in the medium, $S(0)$ is the scattering matrix in the forward direction, and ρ is the number density of MNPs in a suspension. Taking into account the optical theorem [68] for extinction cross section $C_{\text{ext}} = (4\pi/k^2)\text{Re}[S(0)]$, one could write the Beer's law in the following form:

$$I(h) = I(0)\exp(-m_b\rho h C_{\text{ext}}). \tag{7}$$

Finally, the extinction cross section of a spherical nanoparticle is [68]:

$$C_{\text{ext}} = \frac{2\pi}{k^2}\sum_{l=1}^{\infty}(2l+1)\,\text{Re}(a_l + b_l), \tag{8}$$

where a_l and b_l are Mie coefficients which are defined in the Appendix.

2.3. Combined model

We are now ready to consider the *nano*-scale enhancement and *macro*-scale extinction within the one combined model. Let us consider the slab with thickness h of MNPs with concentration $\rho(z)$, which generally depends on the position z of the MNP. The schematic representation of such a system is depicted in Fig. 1(d). Let us assume that the initial pump signal is S_0 and the average number of UC particles attached to MNP is $\langle N\rangle$. The local UC signal at location z is then:

$$S_{\text{loc}}(z) = \langle N\rangle S_0 A f_{\text{loc}}\rho(z)\exp\left[-\int_0^z \text{d}z'\rho(z)m_b C_{\text{ext}}(\omega_{\text{ex}})\right], \tag{9}$$

Optical Materials EXPRESS

where f_{loc} is the local UC enhancement factor defined by Eqs (2) or (4) depending on UC enhancement strategy (excitation or emission enhancement). The first term in Eq. (9) before the exponent describes the local enhancement, while the exponent describes extinction of pump signal at location z. The emitted upconverted signal with frequency ω_{em} attenuates during its propagation through the rest of the slab:

$$S_{\text{uc}} \propto \exp\left[-\int_z^h \mathrm{d}z' \rho(z) m_b C_{\text{ext}}(\omega_{\text{em}})\right]. \tag{10}$$

Combining these two equations, one could get the expression for the overall registered signal:

$$S_{\text{uc}}(z) = \langle N \rangle S_0 A f_{\text{loc}} \int_0^h \mathrm{d}z \rho(z) \exp\left[-\int_0^z \mathrm{d}z' \rho(z') m_b C_{\text{ext}}(\omega_{\text{ex}})\right] \exp\left[-\int_z^h \mathrm{d}z' \rho(z') m_b C_{\text{ext}}(\omega_{\text{em}})\right], \tag{11}$$

where A is the integral over the transverse beam profile normalized to the peak value, the effective transverse area of the beam [47]. Integration of equation (11) over the whole slab h leads to:

$$S_{\text{uc}} = \langle N \rangle S_0 A f_{\text{loc}} \frac{\exp\left[-m_b C_{\text{ext}}(\omega_{\text{ex}}) \rho h\right] - \exp\left[-m_b C_{\text{ext}}(\omega_{\text{em}}) \rho h\right]}{m_b C_{\text{ext}}(\omega_{\text{em}}) - m_b C_{\text{ext}}(\omega_{\text{ex}})}. \tag{12}$$

It can be seen that generally, Eq. (12) is similar to ones obtained for SERS [47] or SE-FSRS [49]. The appropriate value of f_{loc}, however, has to be chosen depending on the actual geometry of the MNP and the regime of UC enhancement by MNP: excitation or emission. Moreover, the large spectral difference between ω_{ex} and ω_{em} implies the predominance of $C_{\text{ext}}(\omega_{\text{ex}})$ or $C_{\text{ext}}(\omega_{\text{em}})$, depending on the UC enhancement regime. Thus, only pump or upconverted signal will experience pronounced extinction while the other one will likely propagate through the slab with negligible attenuation.

2.4. Quantum finite-size effects

Finally, the multilayered MNP geometry represented in Fig. 1(b) implies the use of sufficiently *thin* metal layer. In this case, its bulk frequency-dependent dielectric permittivity $\varepsilon(\omega)$ has to be modified in accordance with quantum finite-size effects [69] which play important role and completely change the optical response of multilayered MNPs with metal thin layers [70,71]. The frequency-dependent tabulated data for bulk $\varepsilon(\omega)$ has to be corrected in the following manner:

$$\varepsilon(\omega) \to \varepsilon(\omega) + \frac{\omega_p^2}{\omega^2 + i\Gamma_{\text{bulk}}\omega} - \frac{\omega_p^2}{\omega^2 + i\Gamma_{\text{fin}}\omega}, \tag{13}$$

where ω_p is the plasma frequency, Γ_{bulk} is the relaxation constant for bulk material, and Γ_{fin} is:

$$\Gamma_{\text{fin}} = \Gamma_{\text{bulk}} + A_L \frac{\upsilon_F}{L_{\text{eff}}}, \tag{14}$$

where υ_F is the Fermi velocity, L_{eff} is the mean free path of conduction electrons and A_L is the dimensionless parameter which is assumed to be unity in most of the cases [68]. There are several ways to define L_{eff} for nanoshells [72], however, setting L_{eff} to be equal to the thickness of a metal shell provides reliable and consistent results [73].

3. Discussion

3.1. UC enhancement by single MNP

We start with *local* UC enhanced by single MNP and limit the discussion with commonly utilized plasmonic materials: Au and Ag. In what follows, we assume that MNPs are embedded

Optical Materials EXPRESS

in water with $m_b = 1.33$. We chose SiO_2 as a spacer layer with constant refractive index 1.54. The refractive index of UC material is assumed to be 1.48. Dielectric constants for Au and Ag are taken from ref [74]. Quantum finite-size effects are introduced via Eq. (13) with the following parameters for Au [75]: $\Gamma_{\text{bulk}}/\omega_p = 0.00253$, $\upsilon_F/c = 0.0046$, and for Ag [75]: $\Gamma_{\text{bulk}}/\omega_p = 0.0019$ and $\upsilon_F/c = 0.0046$, where c is the speed of light in the vacuum.

Although UC core / dielectric spacer / metal shell structures have been already considered as a platform for plasmon-enhanced UC [29, 55–57], there is a lack of information in terms of optimization of the gain in the recorded upconverted signal due to complexity of experiments and high computational costs of exact numerical simulations. However, developed in this paper theory makes it possible to consider wide variety of geometries at almost negligible computational cost.

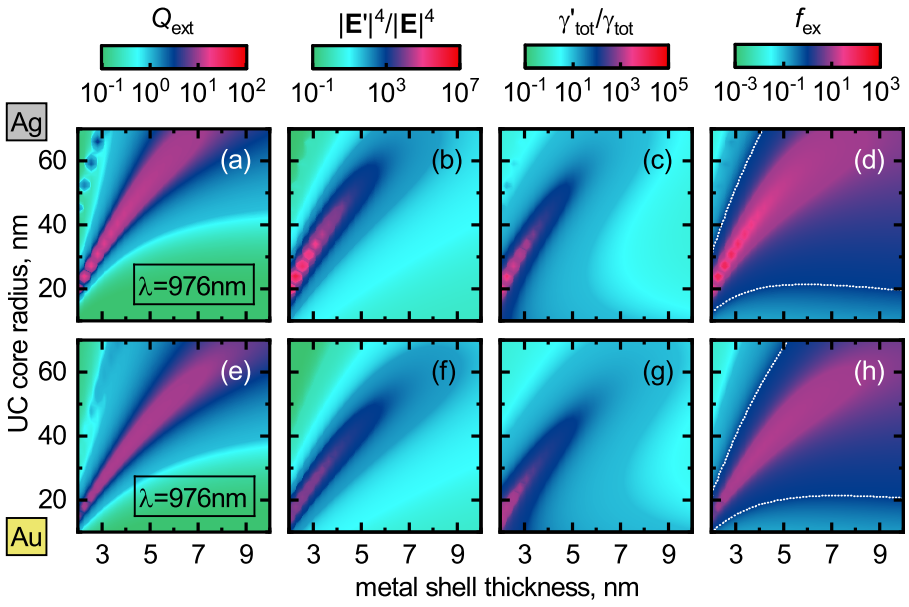

Fig. 2. Extinction efficiency Q_{ext}, electric field enhancement $|\mathbf{E}'|^4/|\mathbf{E}|^4$, total decay rate enhancement $\gamma'_{\text{tot}}/\gamma_{\text{tot}}$, and excitation enhancement f_{ex} for multilayered MNPs: UC core / SiO_2 spacer / metal shell. Shells are chosen to be Ag (top panels) and Au (bottom panels). The thickness of SiO_2 spacer layer is fixed to be 10 nm in all cases. Excitation wavelength is $\lambda_{\text{ex}} = 976$ nm. Dotted lines in right panels correspond to $f_{\text{ex}} = 1$.

Figure 2 shows a comparative analysis of the local field enhancement $|\mathbf{E}'|^4/|\mathbf{E}|^4$ and the total decay rate $\gamma'_{\text{tot}}/\gamma_{\text{tot}}$ enhancement at $\lambda_{\text{ex}} = 976$ nm wavelength in the center of the UC core surrounded by 10 nm thick SiO_2 spacer layer and Ag or Au thin (up to 10 nm) shells. We do not consider SiO_2 spacer layers with different thicknesses, because smaller thickness might be insufficient for successful suppression of UC quenching, while the use of thicker spacer shell will only imply the use of the UC core with smaller size for reaching efficient UC enhancement. The latter trend does not considerably change the f_{ex} values while at the same time it leads to decrease of the volume of UC material in the core of multilayered MNP which is required to keep f_{ex} the same. We also imply that for sufficiently thick SiO_2 spacer layer, electric field distribution as well as total decay rates are almost homogeneous within the UC core, thus, we limit our discussion with the values of $|\mathbf{E}'|^4/|\mathbf{E}|^4$ and $\gamma'_{\text{tot}}/\gamma_{\text{tot}}$ calculated for dipolar emitter located in the center of MNP, which is approximately equal to averaging of all luminescing lanthanides within the UC core. Finally, UC core radius and metal shell thickness have been varied in a wide range of sizes.

It can be seen from Fig. 2 that both $|\mathbf{E}'|^4/|\mathbf{E}|^4$ and $\gamma'_{\text{tot}}/\gamma_{\text{tot}}$ reach the highest values for MNPs

Optical Materials EXPRESS

with almost the same sizes. However, the maximum values of fourth power of the local field enhancement are generally 1-2 orders of magnitude larger than the maximum values of the decay rate enhancement, which results in up to $f_{ex} \approx 150$ and $f_{ex} \approx 20$ UC enhancements for Ag and Au MNPs, respectively. Of note, recently proposed Au nanorods provide up to ≈ 160-fold simultaneous emission-excitation enhancement [32]. Moreover, according to Eq. (12), the actual recorded upconverted signal is proportional to the average number $\langle N \rangle$ of UC particles attached to MNP, or, in other words, to the volume occupied by UC material. From this point of view, multilayered MNPs with UC core seem to be quite promising, because UC process is enhanced equally in whole UC core due to homogeneous electric field distribution inside the core, while, for example, UC enhancement near the nanorod takes place only in spatially shrunk near-field zone with high local field enhancement [26].

Finally, it is insightful to compare the size-dependent local field enhancement with extinction efficiency $Q_{ext} = C_{ext}/(\pi R^2)$, where R is the total radius of the multilayered MNP. It can be seen from Fig. 2 that generally the size of multilayered MNP with highest $|\mathbf{E}'|^4/|\mathbf{E}|^4$ is slightly smaller than the size of multilayered MNP with highest Q_{ext}. Thus, during the fabrication and characterization of MNPs for plasmon-enhanced UC one should keep in mind that the nanostructure with the highest extinction efficiency (which is usually measured in laboratory experiments) does not imply the most efficient excitation enhancement of the UC process.

The plasmonically induced enhancement of UC emission is based on the principle that the MNP is acting as an additional antenna which emits light at frequency ω_{em}. For this purpose, the use of MNPs with $\omega_{LSPR} = \omega_{em}$ seems to be intuitively logical. However, the presence of a dielectric spacer, which is needed for quenching suppression, may significantly change the near- and far-field responses of multilayered MNP [30], thus, the requirement $\omega_{LSPR} = \omega_{em}$ may not be the correct one to reach the highest gain in f_{em}. It is worth to mention that most of theoretical works in the field of plasmon-enhanced UC consider optical properties of MNPs *without* taking into account the presence of the spacer [26, 32], however, it is a well-known fact that even thin SiO_2 layer can significantly change the overall pattern of near-field response of MNPs embedded even in water suspension [30], even though it seems to be 'safe' to neglect the presence of dielectric spacer layer in simulations because its refractive index is almost the same as for surrounding medium.

Figure 3 represents the emission enhancement f_{em} at $\lambda_{em} = 540$ nm and $\lambda_{em} = 650$ nm wavelengths for UC particle located on the surface of Ag core / SiO_2 shell multilayered MNP. Although in real experiments the synthesis of the UC *shell* is the most likely event, for the sake of simplicity we consider UC *particle* with 2 nm radius, which is consistent with experimental data [26]. Such UC particle can be approximated by dipole emitter. This geometry of multilayered MNP perfectly reproduces the actual experimental samples, where the UC material is attached to multilayered MNPs. Moreover, large number of various UC materials utilized in the field of plasmon-enhanced UC [22, 24] may have different initial quantum yield η_0. Therefore, we have discussed a couple of different scenarios ($\eta = 0.1\%, 1\%, 10\%$) to show general features and behavior of UC emission enhancement. It can be seen from Fig. 3 that highest Q_{ext} does not necessarily imply the highest UC enhancement f_{em} at both λ_{em}. While the Q_{ext} reaches its maximum for multilayered MNPs with Ag core radius larger than 50 nm for $\lambda_{em} = 540$ nm and larger than 60 nm for $\lambda_{em} = 650$ nm, emission enhancement f_{em} can reach maximum for multilayered MNPs with smaller Ag core at both wavelengths. This property takes place for each value of initial quantum yield η_0, which implies the usefulness of off-resonance UC emission enhancement for all cases.

It is also worth mentioning that optimal thickness of SiO_2 shell which provides the highest f_{em} depends on the value of η_0. Thus, for $\eta_0 = 0.1\%$, UC material has to be located in the 10 nm vicinity from Ag core, while highly emitting UC material with $\eta_0 = 10\%$ has to be moved away at 10 – 20 nm distance from the metal core. Finally, as expected, Fig. 3 explicitly shows that

Optical Materials EXPRESS

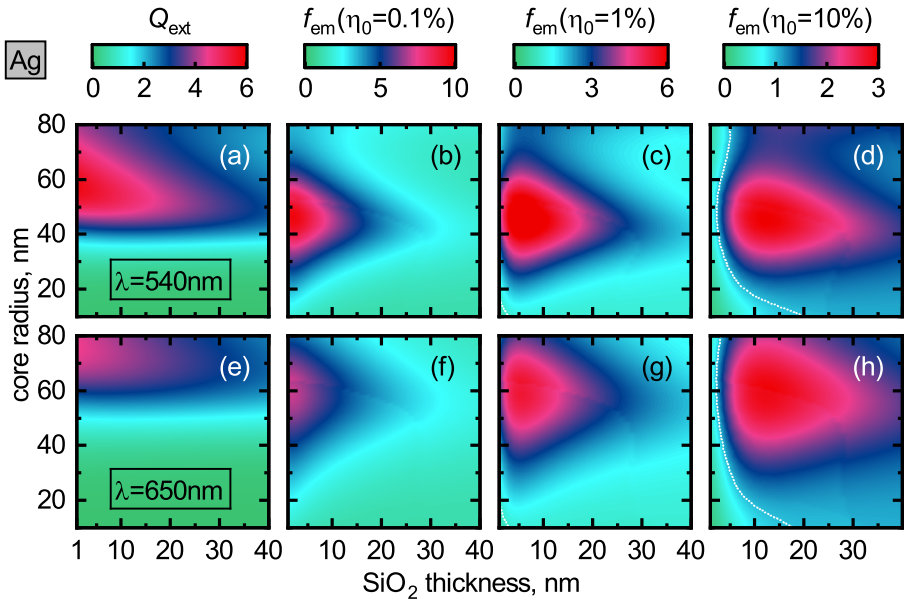

Fig. 3. Extinction efficiency Q_{ext}, and emission enhancement f_{em} for multilayered MNPs with Ag core / SiO_2 shell geometry at two wavelengths: λ = 540 nm (top panels) and λ = 650 nm (bottom panels), and for different initial quantum yields η_0: 0.1%, 1%, 10%. The UC material is located directly on SiO_2 shell, and the distance between the surface of SiO_2 shell and the center of UC particle is 2 nm. Dotted lines correspond to f_{em} = 1.

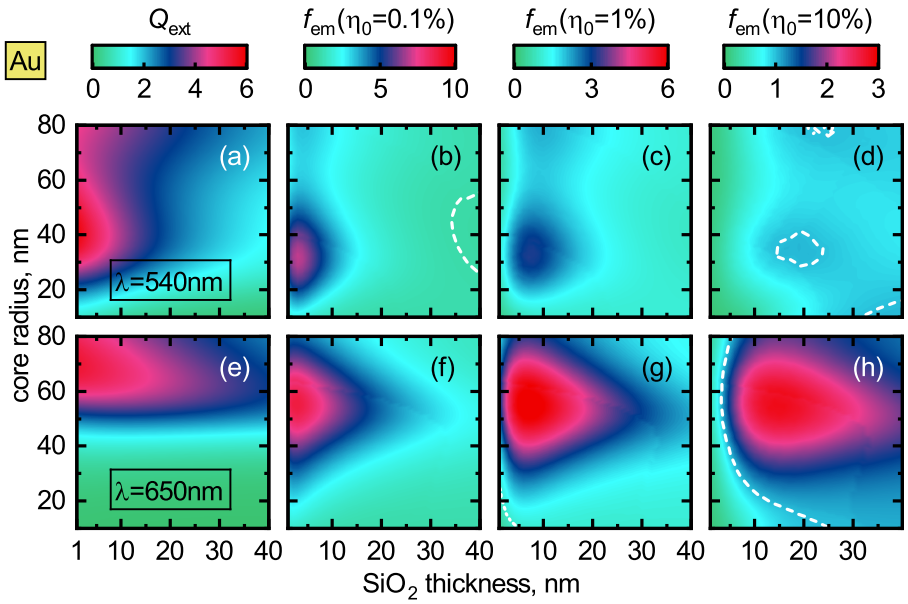

Fig. 4. The same as in Fig. 3, but for multilayered MNPs with Au core / SiO_2 shell geometry.

Optical Materials EXPRESS

the maximum reachable f_{em} is limited with and strongly depends on η_0: emission enhancement gradually decreases for UC materials with higher initial quantum yield. However, in terms of overall plasmonically modified quantum yield η', the configuration with low $f_{em} \approx 3$ and high $\eta_0 = 10\%$ gives the higher quantum yield compared to high $f_{em} \approx 10$ and low $\eta_0 = 0.1\%$: $\eta' \approx 30\%$ vs $\eta' \approx 1\%$. Therefore, even at local scale, the UC emission enhancement is not the appropriate quantity which has to be chosen to characterize registered UC signal.

The UC emission enhancement pattern in Au core / SiO_2 shell multilayered MNPs which is represented in Fig. 4 is qualitative the same for Ag core / SiO_2 shell multilayered MNP which is shown in Fig. 3. However, it can be seen from Fig. 4 that Au is not suitable for UC emission enhancement at $\lambda_{em} = 540$ nm, while the overall f_{em} at $\lambda_{em} = 650$ nm is qualitatively the same, and quantitatively is slightly larger than for Ag core / SiO_2 shell multilayered MNP at the same wavelength.

3.2. UC enhancement and extinction in a slab of MNPs

After the thorough discussion of competition between UC quenching and enhancement by single MNP, it is of particular interest to consider balancing between the extinction of pump signal and UC enhancement in a suspension of plasmonically enhanced UC particles. We start with extinction efficiency Q_{ext} spectra for Ag and Au MNPs optimized for UC excitation enhancement at $\lambda_{ex} = 976$ nm and UC emission enhancement at $\lambda_{em} = 540$ nm and $\lambda_{em} = 650$ nm in accordance with data from Figs. 2-4. We will refer to these MNPs as MNP-1, MNP-2 and MNP-3, respectively. Composition and sizes of each MNP are indicated in Fig. 5 caption.

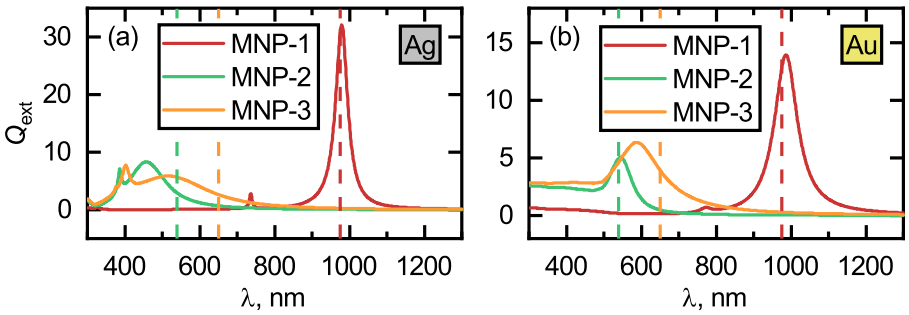

Fig. 5. Extinction efficiency Q_{ext} for MNPs with the following geometry: (a) MNP-1 - three-layered sphere as in Fig. 1(b) with UC core radius 31 nm, SiO_2 spacer thickness 10 nm and Ag shell thickness 3.82 nm, MNP-2 - two-layered sphere as depicted in Fig. 1(c) with Ag core radius 42 nm and SiO_2 shell thickness 3 nm, MNP-3 - the same as MNP-2, but for Ag core with radius 57 nm. (b) MNP-1 - three-layered sphere as in Fig. 1(b) with UC core radius 27 nm, SiO_2 spacer thickness 10 nm and Au shell thickness 3.01 nm, MNP-2 - two-layered sphere as depicted in Fig. 1(c) with Au core radius 33 nm and SiO_2 shell thickness 3 nm, MNP-3 - the same as MNP-2, but for Au core with radius 56 nm. Vertical dashed lines correspond to 540 nm, 650 nm and 976 nm.

It can be seen from Fig. 5 that, as expected, the peak of Q_{ext} is slightly red-shifted with respect to λ_{ex} for MNP-1 for both Ag and Au shells. Peaks of Q_{ext} for MNP-2 and MNP-3 with Ag core are significantly blue-shifted with respect to λ_{em}, while for Au core, optimal configuration of MNP-2 for emission enhancement has the high Q_{ext}. This behavior of multilayered MNPs optical response provides an essential understanding of competition effects during signal propagation through the slab of plasmonically enhanced UC particles. Instead of simultaneously strong extinction of pump and upconverted signals, in most of the cases one should expect strong attenuation of only one of these signals, depending on the UC enhancement regime. Thus, for UC excitation enhancement,

Optical Materials EXPRESS

pump signal at λ_{ex} experiences pronounced decay while upconverted signal propagates with negligible attenuation due to almost zero Q_{ext}, and vice versa for UC emission enhancement. Finally, despite of small decay of upconverted signal during the propagation through the slab of MNPs, one should not expect significantly large recorded upconverted signal due to low values of *local* UC emission enhancement f_{em}. Given the pronounced spectral shift between λ_{ex} and λ_{em}, the off-resonant plasmon-enhanced UC similar to MNP-2 and MNP-3 configuration for Ag, and MNP-3 for Au, represents the most promising strategy due to low extinction at both excitation and emission frequencies.

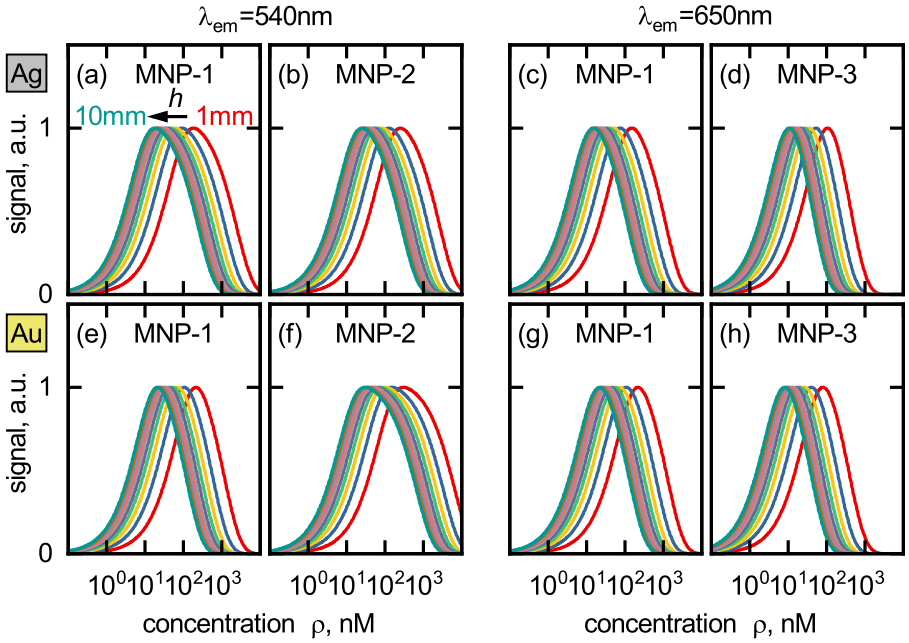

Fig. 6. Normalized upconverted signal in a slab of different Ag (top row) and Au (bottom row) MNPs as a function of concentration ρ measured in transmission mode at λ_{em} = 540 nm and λ_{em} = 650 nm for various values of path length h from 1 mm to 10 mm with 1 mm increment. Calculations are performed with Eq. (12) for solutions of MNP-1, MNP-2 and MNP-3. Initial quantum yield is assumed to be η_0 = 10% in all cases.

Competition between extinction and enhancement implies the interplay between the thickness h of a slab and concentration ρ of MNPs which provides optimal values of ρ_{opt} for each h to reach the highest possible recorded upconverted signal. Figure 6 represents the normalized recorded upconverted signal as a function of concentration ρ for different values of slab thickness h. It can be seen, that, generally, the optimal concentration ρ_{opt} varies from $\approx$ 10 nM to $\approx$ 200 nM for slab with thickness from 10 mm to 1 mm, respectively. Au MNPs optimized both for UC excitation enhancement at λ_{ex} = 976 nm and UC emission enhancement at λ_{em} = 540 nm and λ_{em} = 650 nm reveal the qualitatively the same behavior as Ag MNPs, which can be seen from Figs. 6(e)-6(h). However, optimal concentrations ρ_{opt} are generally $\approx$ 1.5 – 2 times larger than corresponding ρ_{opt} for Ag MNPs, which is explained by weaker extinction of pump and upconverted signals due to lower Q_{ext} for Au MNPs. According to previously reported results for SERS [47] and SE-FSRS [49], the existence of ρ_{opt} is justified by the balancing of extinction in the slab by strong enhancement from MNPs. The expression for ρ_{opt} can be easily found by setting the derivative of Eq. (12) to zero [49]. Finally, the decreasing of ρ_{opt} for thicker slabs is explained by increased optical path, and, as a consequence, larger extinction. Thus, for fixed f_{loc},

Optical Materials EXPRESS

one have to decrease ρ to minimize extinction and balance it by enhancement effects.

4. Conclusion

To conclude, we have developed comprehensive and self-consistent theory which describes the UC enhancement in single multilayered metallodielectric spherical nanoparticle, and in their suspensions. Classical decay rates of dipole emitter and electric field enhancement in the presence of multilayered spherical nanoparticle are found within the framework of extended Mie theory, while extinction of pump and upconverted signals are defined from effective medium approach.

We have thoroughly analyzed the competition between the UC enhancement and quenching both *locally*, near the single plasmonic nanoparticle, and *macroscopically*, in suspension of such nanoparticles. This work provides general guidelines for synthesizing plasmonically enhanced upconversion nanoparticles with the highest possible upconversion enhancement. The balancing effects at both scales imply the existence of optimal *local* and *macroscopic* parameters to reach the stronger recorded upconverted signal. We point out to the fact that commonly considered *local* figures of merit f_{ex} and f_{em} as defined by Eq. (2) and (4), respectively, are not the appropriate quantities that have to be optimized to get the maximum recorded upconverted signal from *macroscopic* slab of plasmonically enhanced UC particles.

We show, that the optimal geometry of multilayered MNP for *local* UC excitation enhancement at $\lambda_{\text{ex}} = 976$ nm is: UC core with < 30 nm radius / ≈ 10 nm SiO_2 spacer layer / thin < 5 nm metal (either Ag or Au) shell. While for *local* UC emission enhancement at $\lambda_{\text{em}} = 540$ nm and $\lambda_{\text{em}} = 650$ nm, the optimal parameters are: $\approx 40 - 60$ metal core and $1 - 20$ nm SiO_2 spacer shell, which thickness strongly depends on the initial quantum yield η_0 of UC material, i.e. UC particles with higher η_0 have to be located farther from metal core compared to UC particles with lower η_0. As for *macroscopic* propagation of the upconverted signal, the optimal concentration of MNPs in a suspension varies from ≈ 10 nM to ≈ 200 nM for Ag MNPs, depending on the thickness of the slab, and ρ is $\approx 1.5 - 2$ larger for Au MNPs.

Developed theoretical model considers only steady-state excitation of the UC process, which implies the constant temperature of MNPs, and, as a consequence, the neglect of heating effects. However, pulsed laser irradiation inevitably heats MNPs [60] and changes their optical response [76]. Moreover, the influence of MNPs on local density of states of UC material may also affect the UC process [35, 36]. Finally, although we have limited the discussion with MNPs from classic plasmonic materials such as Ag and Au, developed theory can be applied for rapidly emerging field of semiconductor nanoparticles [44, 77–79] or alternative plasmonic materials [80–83]. Incorporating thermal effects and modification of local density of states into reported theoretical treatment, as well as the use of alternative plasmonic materials are out of the scope of this paper, however, they represent promising directions which may result in further optimization of plasmon-enhanced upconversion.

Appendix

Let us consider a multilayered sphere which consists of N layers and is embedded in a non-absorbing homogeneous environment with purely real refractive index $m_b = m_{N+1}$ as depicted in Fig. 7. For the convenience, the surrounding medium is also considered as a layer with $N + 1$ index. Decay rates, local field enhancement and extinction cross section of such a particle can be evaluated within the framework of Mie theory [68] with the extension to multilayered sphere [61].

We set the permeability $\mu_j = 1$ for each j-th layer including background medium. In this case, j-th layer is coupled with $(j + 1)$-th layer with the following electric (E) and magnetic (M) forward (+) and backward (−) transfer matrices [61]:

Optical Materials EXPRESS

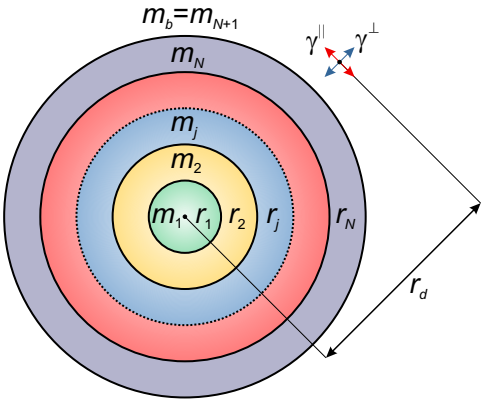

Fig. 7. Schematic representation of the multilayered spherical particle with N layers embedded in a host medium with m_b.

$$T^{-}_{Ml}(j) = -\mathrm{i}\begin{pmatrix} \xi_l'(k_j r_j)\psi_l(k_{j+1} r_j)/\overline{m}_{j+1} - \xi_l(k_j r_j)\psi_l'(k_{j+1} r_j) & \xi_l'(k_j r_j)\xi_l(k_{j+1} r_j)/\overline{m}_{j+1} - \xi_l(k_j r_j)\xi_l'(k_{j+1} r_j) \\ -\psi_l'(k_j r_j)\psi_l(k_{j+1} r_j)/\overline{m}_{j+1} + \psi_l(k_j r_j)\psi_l'(k_{j+1} r_j) & -\psi_l'(k_j r_j)\xi_l(k_{j+1} r_j)/\overline{m}_{j+1} + \psi_l(k_j r_j)\xi_l'(k_{j+1} r_j) \end{pmatrix} \tag{15}$$

$$T^{+}_{Ml}(j) = -\mathrm{i}\begin{pmatrix} \overline{m}_{j+1}\xi_l'(k_{j+1} r_j)\psi_l(k_j r_j) - \xi_l(k_{j+1} r_j)\psi_l'(k_j r_j) & \overline{m}_{j+1}\xi_l'(k_{j+1} r_j)\xi_l(k_j r_j) - \xi_l(k_{j+1} r_j)\xi_l'(k_j r_j) \\ -\overline{m}_{j+1}\psi_l'(k_{j+1} r_j)\psi_l(k_j r_j) + \psi_l(k_{j+1} r_j)\psi_l'(k_j r_j) & -\overline{m}_{j+1}\psi_l'(k_{j+1} r_j)\xi_l(k_j r_j) + \psi_l(k_{j+1} r_j)\xi_l'(k_j r_j) \end{pmatrix} \tag{16}$$

$$T^{-}_{El}(j) = -\mathrm{i}\begin{pmatrix} \xi_l'(k_j r_j)\psi_l(k_{j+1} r_j) - \xi_l(k_j r_j)\psi_l'(k_{j+1} r_j)/\overline{m}_{j+1} & \xi_l'(k_j r_j)\xi_l(k_{j+1} r_j) - \xi_l(k_j r_j)\xi_l'(k_{j+1} r_j)/\overline{m}_{j+1} \\ -\psi_l'(k_j r_j)\psi_l(k_{j+1} r_j) + \psi_l(k_j r_j)\psi_l'(k_{j+1} r_j)/\overline{m}_{j+1} & -\psi_l'(k_j r_j)\xi_l(k_{j+1} r_j) + \psi_l(k_j r_j)\xi_l'(k_{j+1} r_j)/\overline{m}_{j+1} \end{pmatrix} \tag{17}$$

$$T^{+}_{El}(j) = -\mathrm{i}\begin{pmatrix} \xi_l'(k_{j+1} r_j)\psi_l(k_j r_j) - \overline{m}_{j+1}\xi_l(k_{j+1} r_j)\psi_l'(k_j r_j) & \xi_l'(k_{j+1} r_j)\xi_l(k_j r_j) - \overline{m}_{j+1}\xi_l(k_{j+1} r_j)\xi_l'(k_j r_j) \\ -\psi_l'(k_{j+1} r_j)\psi_l(k_j r_j) + \overline{m}_{j+1}\psi_l(k_{j+1} r_j)\psi_l'(k_j r_j) & -\psi_l'(k_{j+1} r_j)\xi_l(k_j r_j) + \overline{m}_{j+1}\psi_l(k_{j+1} r_j)\xi_l'(k_j r_j), \end{pmatrix} \tag{18}$$

where $\mathrm{i} = \sqrt{-1}$, $k_j = 2\pi m_j/\lambda$ is the wavenumber in j-th layer, $\overline{m}_{j+1} = m_{j+1}/m_j$ is the refractive index of the $(j+1)$-th layer with respect to the j-th layer, and Ricatti-Bessel functions $\psi_n(z) = z j_l(z)$ and $\xi_l(z) = z h_l^{(1)}(z)$ are introduced for the convenience, where j_l and $h_l^{(1)}$ are the spherical Bessel and Hankel (of the first kind) functions. The prime denotes differentiation with respect to the argument in parentheses, and index j runs from 1 to N.

Next, it is convenient to introduce the following forward and backward matrices:

$$\mathscr{T}_{Ml}(n) = \prod_{j=1}^{n-1} T^{+}_{Ml}(j), \qquad \mathscr{M}_{Ml}(n) = \prod_{j=n}^{N} T^{-}_{Ml}(j), \tag{19}$$

$$\mathscr{T}_{El}(n) = \prod_{j=1}^{n-1} T^{+}_{El}(j), \qquad \mathscr{M}_{El}(n) = \prod_{j=n}^{N} T^{-}_{El}(j). \tag{20}$$

These matrices are transfer expansion coefficients from the sphere core (for $\mathscr{T}(n)$) and surrounding medium (for $\mathscr{M}(n)$) to the nth layer. Thus, Mie coefficients a_l and b_l from Eq. (8) can be found as:

Optical Materials EXPRESS

$$a_l = -\mathscr{T}_{21;El}(N+1)/\mathscr{T}_{11;El}(N+1), \tag{21}$$
$$b_l = -\mathscr{T}_{21;Ml}(N+1)/\mathscr{T}_{11;Ml}(N+1). \tag{22}$$

The mean radiative and nonradiative decay rates of dipole emitter located near the multilayered sphere are found by the geometrical averaging of corresponding radial and tangential components (see Fig. 7):

$$\frac{\gamma_{\mathrm{rad,nrad}}}{\gamma_0} = \frac{\gamma^{\perp}_{\mathrm{rad,nrad}} + 2\gamma^{\parallel}_{\mathrm{rad,nrad}}}{3\gamma_0}, \tag{23}$$

where γ_0 is the decay rate of dipole emitter in free space.

Radial ($\perp$) and tangential ($\parallel$) components of radiative and nonradiative decay rates for dipole emitter located *outside* of the multilayered sphere (i.e. $r_d > r_N$):

$$\frac{\gamma^{\perp}_{\mathrm{rad}}}{\gamma_0} = \frac{3}{2(k_b r_d)^4}\sum_l l(l+1)(2l+1)\left|\psi_l(k_b r_d) + \frac{\mathscr{T}_{21;El}}{\mathscr{T}_{11;El}}\xi_l(k_b r_d)\right|^2, \tag{24}$$

$$\frac{\gamma^{\parallel}_{\mathrm{rad}}}{\gamma_0} = \frac{3}{4(k_b r)^2}\sum_l (2l+1)\left[\left|\psi_l(k_b r_d) + \frac{\mathscr{T}_{21;Ml}}{\mathscr{T}_{11;Ml}}\xi_l(k_b r_d)\right|^2 + \left|\psi_l'(k_h r_d) + \frac{\mathscr{T}_{21;El}}{\mathscr{T}_{11;El}}\xi_l'(k_b r_d)\right|^2\right], \tag{25}$$

$$\frac{\gamma^{\perp}_{\mathrm{nrad}}}{\gamma_0} = \frac{3k_b^3}{2(k_b r_d)^4}\frac{1}{m_b^2}\mathrm{Im}[m_a^2]\sum_l l(l+1)(2l+1)I_{El}\left|\xi_l(k_b r_d)\right|^2, \tag{26}$$

$$\frac{\gamma^{\parallel}_{\mathrm{nrad}}}{\gamma_0} = \frac{3k_h^3}{4(k_b r_d)^2}\frac{1}{m_b^2}\mathrm{Im}[m_a^2]\sum_l (2l+1)\left[I_{Ml}\left|\xi_l(k_b r_d)\right|^2 + I_{El}\left|\xi_l'(k_b r_d)\right|^2\right], \tag{27}$$

and *inside* the sphere core, (i.e. $r_d < r_1$):

$$\frac{\gamma^{\perp}_{\mathrm{rad}}}{\gamma_0} = \frac{3}{2(k_1 r_d)^4}\frac{m_1}{m_b}\sum_l l(l+1)(2l+1)\left|\frac{\psi_l(k_1 r_d)}{\mathscr{M}_{22;El}(1)}\right|^2, \tag{28}$$

$$\frac{\gamma^{\parallel}_{\mathrm{rad}}}{\gamma_0} = \frac{3}{4(k_1 r_d)^2}\frac{m_1}{m_b}\sum_l (2l+1)\left[\left|\frac{\psi_l(k_1 r_d)}{\mathscr{M}_{22;Ml}(1)}\right|^2 + \left|\frac{\psi_l'(k_1 r_d)}{\mathscr{M}_{22;El}(1)}\right|^2\right], \tag{29}$$

$$\frac{\gamma^{\perp}_{\mathrm{nrad}}}{\gamma_0} = \frac{3k_1^3}{2(k_1 r_d)^4}\frac{1}{m_1^2}\mathrm{Im}[m_a^2]\sum_l l(l+1)(2l+1)I_{El}\left|\frac{\psi_l(k_1 r_d)}{\mathscr{M}_{22;El}(1)}\right|^2, \tag{30}$$

$$\frac{\gamma^{\parallel}_{\mathrm{nrad}}}{\gamma_0} = \frac{3k_1^3}{4(k_1 r_d)^2}\frac{1}{m_1^2}\mathrm{Im}[m_a^2]\sum_l (2l+1)\left[I_{Ml}\left|\frac{\psi_l(k_1 r_d)}{\mathscr{M}_{22;Ml}(1)}\right|^2 + I_{El}\left|\frac{\psi_l'(k_1 r_d)}{\mathscr{M}_{22;El}(1)}\right|^2\right], \tag{31}$$

where $I_{El} = I^{(1)}_{El} + I^{(2)}_{El}$, and

$$I_{Ml} = \frac{1}{|k_a|^2}\int_a \left|a_{Ml}\psi_l(k_a r) + b_{Ml}\xi_l(k_a r)\right|^2 \mathrm{d}r, \tag{32}$$

$$I^{(1)}_{El} = \frac{l(l+1)}{|k_a|^4}\int_a \left|a_{El}\psi_l(k_a r) + b_{El}\xi_l(k_a r)\right|^2 \frac{\mathrm{d}r}{r^2}, \tag{33}$$

$$I^{(2)}_{El} = \frac{1}{|k_a|^2}\int_a \left|a_{El}\psi_l'(k_a r) + b_{El}\xi_l'(k_a r)\right|^2 \mathrm{d}r. \tag{34}$$

Optical Materials EXPRESS

Here $\int_a$ denotes the radial integration over the shell with a nonzero imaginary part of the refractive index $\mathrm{Im}[m_a] \neq 0$.

Coefficients $a_{\beta l}$ and $b_{\beta l}$, where subscript β stands either for E or M, are defined for dipole located *outside* of the sphere (i.e. $r_d > r_N$) are defined as:

$$a_{\beta l} = \mathscr{M}_{11;\beta l}(l_a) + \mathscr{M}_{12;\beta l}(l_a)\mathscr{T}_{21;\beta l}(N+1)/\mathscr{T}_{11;\beta l}(N+1), \tag{35}$$

$$b_{\beta l} = \mathscr{M}_{21;\beta l}(l_a) + \mathscr{M}_{22;\beta l}(l_a)\mathscr{T}_{21;\beta l}(N+1)/\mathscr{T}_{11;\beta l}(N+1), \tag{36}$$

and *inside* the sphere core, (i.e. $r_d < r_1$):

$$a_{\beta l} = \mathscr{M}_{12;\beta l}(l_a), \tag{37}$$

$$b_{\beta l} = \mathscr{M}_{22;\beta l}(l_a), \tag{38}$$

where l_a is the index of the absorbing shell.

Finally, total decay rate γ_{tot} will read:

$$\frac{\gamma_{\mathrm{tot}}}{\gamma_0} = \frac{\gamma_{\mathrm{rad}}}{\gamma_0} + \frac{\gamma_{\mathrm{nrad}}}{\gamma_0}, \tag{39}$$

and the commonly utilized criterion for upper limit l_{max} of summations in above equations is

$$l_{\mathrm{max}} = (k_1 r_d) + 4.05(k_1 r_d)^{1/3} + 2, \tag{40}$$

which, however, may vary for each particular case of interest [84].

Funding

National Science Foundation (NSF) (CHE-1503408).

References

1. F. Auzel, "Upconversion and Anti-Stokes Processes with f and d Ions in Solids," Chem. Rev. **104**, 139–174 (2004).
2. B. Zhou, B. Shi, D. Jin, and X. Liu, "Controlling upconversion nanocrystals for emerging applications," Nat. Nanotechnol. **10**, 924–936 (2015).
3. G. Chen, H. Qiu, P. N. Prasad, and X. Chen, "Upconversion Nanoparticles: Design, Nanochemistry, and Applications in Theranostics," Chem. Rev. **114**, 5161–5214 (2014).
4. C.-W. Chen, P.-H. Lee, Y.-C. Chan, M. Hsiao, C.-H. Chen, P. C. Wu, P. R. Wu, D. P. Tsai, D. Tu, X. Chen, and R.-S. Liu, "Plasmon-induced hyperthermia: hybrid upconversion NaYF 4 :Yb/Er and gold nanomaterials for oral cancer photothermal therapy," J. Mater. Chem. B **3**, 8293–8302 (2015).
5. L. Zhou, R. Wang, C. Yao, X. Li, C. Wang, X. Zhang, C. Xu, A. Zeng, D. Zhao, and F. Zhang, "Single-band upconversion nanoprobes for multiplexed simultaneous in situ molecular mapping of cancer biomarkers," Nat. Commun. **6**, 6938 (2015).
6. X. Wu, Y. Zhang, K. Takle, O. Bilsel, Z. Li, H. Lee, Z. Zhang, D. Li, W. Fan, C. Duan, E. M. Chan, C. Lois, Y. Xiang, and G. Han, "Dye-Sensitized Core/Active Shell Upconversion Nanoparticles for Optogenetics and Bioimaging Applications," ACS Nano **10**, 1060–1066 (2016).
7. F. Wang, S. Wen, H. He, B. Wang, Z. Zhou, O. Shimoni, and D. Jin, "Microscopic inspection and tracking of single upconversion nanoparticles in living cells," Light. Sci. & Appl. **7**, 18007 (2018).
8. L. Huot, P. M. Moselund, P. Tidemand-Lichtenberg, L. Leick, and C. Pedersen, "Upconversion imaging using an all-fiber supercontinuum source," Opt. Lett. **41**, 2466 (2016).
9. J. Wang, T. Ming, Z. Jin, J. Wang, L.-D. Sun, and C.-H. Yan, "Photon energy upconversion through thermal radiation with the power efficiency reaching 16%," Nat. Commun. **5**, 5669 (2014).
10. Y. H. Jang, Y. J. Jang, S. Kim, L. N. Quan, K. Chung, and D. H. Kim, "Plasmonic Solar Cells: From Rational Design to Mechanism Overview," Chem. Rev. **116**, 14982–15034 (2016).
11. F. Meng, Y. Luo, Y. Zhou, J. Zhang, Y. Zheng, G. Cao, and X. Tao, "Integrated plasmonic and upconversion starlike Y2O3:Er/Au@TiO2 composite for enhanced photon harvesting in dye-sensitized solar cells," J. Power Sources **316**, 207–214 (2016).
12. D. Li, H. Ågren, and G. Chen, "Near infrared harvesting dye-sensitized solar cells enabled by rare-earth upconversion materials," Dalton Transactions **47**, 8526–8537 (2018).

Optical Materials EXPRESS

13. Y. Liu, Y. Lu, X. Yang, X. Zheng, S. Wen, F. Wang, X. Vidal, J. Zhao, D. Liu, Z. Zhou, C. Ma, J. Zhou, J. A. Piper, P. Xi, and D. Jin, "Amplified stimulated emission in upconversion nanoparticles for super-resolution nanoscopy," Nature **543**, 229–233 (2017).
14. Q. Zhan, H. Liu, B. Wang, Q. Wu, R. Pu, C. Zhou, B. Huang, X. Peng, H. Ågren, and S. He, "Achieving high-efficiency emission depletion nanoscopy by employing cross relaxation in upconversion nanoparticles," Nat. Commun. **8**, 1058 (2017).
15. X. Li, F. Zhang, and D. Zhao, "Highly efficient lanthanide upconverting nanomaterials: Progresses and challenges," Nano Today **8**, 643–676 (2013).
16. W. Zou, C. Visser, J. A. Maduro, M. S. Pshenichnikov, and J. C. Hummelen, "Broadband dye-sensitized upconversion of near-infrared light," Nat. Photonics **6**, 560–564 (2012).
17. J. Zhao, S. Ji, and H. Guo, "Triplet-triplet annihilation based upconversion: from triplet sensitizers and triplet acceptors to upconversion quantum yields," RSC Adv. **1**, 937 (2011).
18. Y. C. Simon and C. Weder, "Low-power photon upconversion through triplet-triplet annihilation in polymers," J. Mater. Chem. **22**, 20817 (2012).
19. J. Zhao, D. Jin, E. P. Schartner, Y. Lu, Y. Liu, A. V. Zvyagin, L. Zhang, J. M. Dawes, P. Xi, J. A. Piper, E. M. Goldys, and T. M. Monro, "Single-nanocrystal sensitivity achieved by enhanced upconversion luminescence," Nat. Nanotechnol. **8**, 729–734 (2013).
20. D. J. Garfield, N. J. Borys, S. M. Hamed, N. A. Torquato, C. A. Tajon, B. Tian, B. Shevitski, E. S. Barnard, Y. D. Suh, S. Aloni, J. B. Neaton, E. M. Chan, B. E. Cohen, and P. J. Schuck, "Enrichment of molecular antenna triplets amplifies upconverting nanoparticle emission," Nat. Photonics **12**, 402–407 (2018).
21. J. Zhou, S. Wen, J. Liao, C. Clarke, S. A. Tawfik, W. Ren, C. Mi, F. Wang, and D. Jin, "Activation of the surface dark-layer to enhance upconversion in a thermal field," Nat. Photonics **12**, 154–158 (2018).
22. D. M. Wu, A. García-Etxarri, A. Salleo, and J. A. Dionne, "Plasmon-Enhanced Upconversion," The J. Phys. Chem. Lett. **5**, 4020–4031 (2014).
23. W. Park, D. Lu, and S. Ahn, "Plasmon enhancement of luminescence upconversion," Chem. Soc. Rev. **44**, 2940–2962 (2015).
24. W. Xu, X. Chen, and H. Song, "Upconversion manipulation by local electromagnetic field," Nano Today **17**, 54–78 (2017).
25. S. Lal, S. Link, and N. J. Halas, "Nano-optics from sensing to waveguiding," Nat. Photonics **1**, 641–648 (2007).
26. Q. Zhan, X. Zhang, Y. Zhao, J. Liu, and S. He, "Tens of thousands-fold upconversion luminescence enhancement induced by a single gold nanorod," Laser & Photonics Rev. **9**, 479–487 (2015).
27. J. R. Lakowicz, "Radiative decay engineering 5: metal-enhanced fluorescence and plasmon emission," Anal. Biochem. **337**, 171–194 (2005).
28. P. Yuan, Y. H. Lee, M. K. Gnanasammandhan, Z. Guan, Y. Zhang, and Q.-H. Xu, "Plasmon enhanced upconversion luminescence of NaYF4:Yb,Er@SiO2@Ag core-shell nanocomposites for cell imaging," Nanoscale **4**, 5132 (2012).
29. Z. Wang, W. Gao, R. Wang, J. Shao, Q. Han, C. Wang, J. Zhang, T. Zhang, J. Dong, and H. Zheng, "Influence of SiO2 layer on the plasmon quenched upconversion luminescence emission of core-shell NaYF4:Yb,Er@SiO2@Ag nanocomposites," Mater. Res. Bull. **83**, 515–521 (2016).
30. J. L. Montaño-Priede, O. Peña-Rodríguez, and U. Pal, "Near-Electric-Field Tuned Plasmonic Au@SiO 2 and Ag@SiO 2 Nanoparticles for Efficient Utilization in Luminescence Enhancement and Surface-Enhanced Spectroscopy," The J. Phys. Chem. C **121**, 23062–23071 (2017).
31. N. S. Abadeer, M. R. Brennan, W. L. Wilson, and C. J. Murphy, "Distance and Plasmon Wavelength Dependent Fluorescence of Molecules Bound to Silica-Coated Gold Nanorods," ACS Nano **8**, 8392–8406 (2014).
32. X. Liu and D. Yuan Lei, "Simultaneous excitation and emission enhancements in upconversion luminescence using plasmonic double-resonant gold nanorods," Sci. Reports **5**, 15235 (2015).
33. P. Alonso-González, P. Albella, F. Neubrech, C. Huck, J. Chen, F. Golmar, F. Casanova, L. E. Hueso, A. Pucci, J. Aizpurua, and R. Hillenbrand, "Experimental Verification of the Spectral Shift between Near- and Far-Field Peak Intensities of Plasmonic Infrared Nanoantennas," Phys. Rev. Lett. **110**, 203902 (2013).
34. R. Esteban, M. Laroche, and J.-J. Greffet, "Influence of metallic nanoparticles on upconversion processes," J. Appl. Phys. **105**, 033107 (2009).
35. S. Fischer, F. Hallermann, T. Eichelkraut, G. von Plessen, K. W. Krämer, D. Biner, H. Steinkemper, M. Hermle, and J. C. Goldschmidt, "Plasmon enhanced upconversion luminescence near gold nanoparticles - simulation and analysis of the interactions," Opt. Express **20**, 271 (2012).
36. S. Fischer, F. Hallermann, T. Eichelkraut, G. von Plessen, K. W. Krämer, D. Biner, H. Steinkemper, M. Hermle, and J. C. Goldschmidt, "Plasmon enhanced upconversion luminescence near gold nanoparticles - simulation and analysis of the interactions: Errata," Opt. Express **21**, 10606 (2013).
37. Y. Ding, X. Zhang, H. Gao, S. Xu, C. Wei, and Y. Zhao, "Plasmonic enhanced upconversion luminescence of β-NaYF4:Yb3+/Er3+ with Ag@SiO2 core-shell nanoparticles," J. Lumin. **147**, 72–76 (2014).
38. Y.-L. Wang, N. Mohammadi Estakhri, A. Johnson, H.-Y. Li, L.-X. Xu, Z. Zhang, A. Alù, Q.-Q. Wang, and C.-K. K. Shih, "Tailoring Plasmonic Enhanced Upconversion in Single NaYF4:Yb3+/Er3+ Nanocrystals," Sci. Reports **5**, 10196 (2015).
39. M. Saboktakin, X. Ye, S. J. Oh, S.-H. Hong, A. T. Fafarman, U. K. Chettiar, N. Engheta, C. B. Murray, and C. R. Kagan, "Metal-Enhanced Upconversion Luminescence Tunable through Metal Nanoparticle-Nanophosphor

Optical Materials EXPRESS

Separation," ACS Nano **6**, 8758–8766 (2012).
40. W. Xu, S. Xu, Y. Zhu, T. Liu, X. Bai, B. Dong, L. Xu, and H. Song, "Ultra-broad plasma resonance enhanced multicolor emissions in an assembled Ag/NaYF4:Yb,Er nano-film," Nanoscale **4**, 6971 (2012).
41. Q.-C. Sun, H. Mundoor, J. C. Ribot, V. Singh, I. I. Smalyukh, and P. Nagpal, "Plasmon-Enhanced Energy Transfer for Improved Upconversion of Infrared Radiation in Doped-Lanthanide Nanocrystals," Nano Lett. **14**, 101–106 (2014).
42. A. L. Feng, M. L. You, L. Tian, S. Singamaneni, M. Liu, Z. Duan, T. J. Lu, F. Xu, and M. Lin, "Distance-Dependent Plasmon-Enhanced Fluorescence of Upconversion Nanoparticles using Polyelectrolyte Multilayers as Tunable Spacers," Sci. Reports **5**, 7779 (2015).
43. Z. Yin, D. Zhou, W. Xu, S. Cui, X. Chen, H. Wang, S. Xu, and H. Song, "Plasmon-Enhanced Upconversion Luminescence on Vertically Aligned Gold Nanorod Monolayer Supercrystals," ACS Appl. Mater. & Interfaces **8**, 11667–11674 (2016).
44. D. Zhou, D. Liu, W. Xu, Z. Yin, X. Chen, P. Zhou, S. Cui, Z. Chen, and H. Song, "Observation of Considerable Upconversion Enhancement Induced by Cu 2- x S Plasmon Nanoparticles," ACS Nano **10**, 5169–5179 (2016).
45. J. Li, Z. Yang, Z. Chai, J. Qiu, and Z. Song, "Preparation and upconversion emission enhancement of SiO_2 coated YbPO_4: Erˆ3+ inverse opals with Ag nanoparticles," Opt. Mater. Express **7**, 3503 (2017).
46. B. Shao, Z. Yang, J. Li, J. Yang, Y. Wang, J. Qiu, and Z. Song, "Upconversion emission enhancement by porous silver films with ultra-broad plasmon absorption," Opt. Mater. Express **7**, 1188 (2017).
47. T. van Dijk, S. T. Sivapalan, B. M. DeVetter, T. K. Yang, M. V. Schulmerich, C. J. Murphy, R. Bhargava, and P. S. Carney, "Competition Between Extinction and Enhancement in Surface-Enhanced Raman Spectroscopy," The J. Phys. Chem. Lett. **4**, 1193–1196 (2013).
48. S. T. Sivapalan, B. M. DeVetter, T. K. Yang, T. van Dijk, M. V. Schulmerich, P. S. Carney, R. Bhargava, and C. J. Murphy, "Off-Resonance Surface-Enhanced Raman Spectroscopy from Gold Nanorod Suspensions as a Function of Aspect Ratio: Not What We Thought," ACS Nano **7**, 2099–2105 (2013).
49. B. X. K. Chng, T. van Dijk, R. Bhargava, and P. S. Carney, "Enhancement and extinction effects in surface-enhanced stimulated Raman spectroscopy," Phys. Chem. Chem. Phys. **17**, 21348–21355 (2015).
50. N. L. Gruenke, M. O. McAnally, G. C. Schatz, and R. P. Van Duyne, "Balancing the Effects of Extinction and Enhancement for Optimal Signal in Surface-Enhanced Femtosecond Stimulated Raman Spectroscopy," The J. Phys. Chem. C **120**, 29449–29454 (2016).
51. D. Lu, S. K. Cho, S. Ahn, L. Brun, C. J. Summers, and W. Park, "Plasmon Enhancement Mechanism for the Upconversion Processes in NaYF 4 :Yb 3+ ,Er 3+ Nanoparticles: Maxwell versus Förster," ACS Nano **8**, 7780–7792 (2014).
52. X. Wang, R. R. Valiev, T. Y. Ohulchanskyy, H. Ågren, C. Yang, and G. Chen, "Dye-sensitized lanthanide-doped upconversion nanoparticles," Chem. Soc. Rev. **46**, 4150–4167 (2017).
53. X. Chen, D. Zhou, W. Xu, J. Zhu, G. Pan, Z. Yin, H. Wang, Y. Zhu, C. Shaobo, and H. Song, "Fabrication of Au-Ag nanocage@NaYF4@NaYF4:Yb,Er Core-Shell Hybrid and its Tunable Upconversion Enhancement," Sci. Reports **7**, 41079 (2017).
54. L. R. Hirsch, R. J. Stafford, J. A. Bankson, S. R. Sershen, B. Rivera, R. E. Price, J. D. Hazle, N. J. Halas, and J. L. West, "Nanoshell-mediated near-infrared thermal therapy of tumors under magnetic resonance guidance," Proc. Natl. Acad. Sci. **100**, 13549–13554 (2003).
55. H. Zhang, Y. Li, I. A. Ivanov, Y. Qu, Y. Huang, and X. Duan, "Plasmonic Modulation of the Upconversion Fluorescence in NaYF4:Yb/Tm Hexaplate Nanocrystals Using Gold Nanoparticles or Nanoshells," Angewandte Chemie Int. Ed. **49**, 2865–2868 (2010).
56. H. Xing, W. Bu, S. Zhang, X. Zheng, M. Li, F. Chen, Q. He, L. Zhou, W. Peng, Y. Hua, and J. Shi, "Multifunctional nanoprobes for upconversion fluorescence, MR and CT trimodal imaging," Biomaterials **33**, 1079–1089 (2012).
57. P. Kannan, F. A. Rahim, X. Teng, R. Chen, H. Sun, L. Huang, and D.-H. Kim, "Enhanced emission of NaYF4:Yb,Er/Tm nanoparticles by selective growth of Au and Ag nanoshells," RSC Adv. **3**, 7718 (2013).
58. Y. Qin, Z. Dong, D. Zhou, Y. Yang, X. Xu, and J. Qiu, "Modification on populating paths of β-NaYF_4:Nd/Yb/Ho@SiO_2@Ag core/double-shell nanocomposites with plasmon enhanced upconversion emission," Opt. Mater. Express **6**, 1942 (2016).
59. A. K. Kodali, X. Llora, and R. Bhargava, "Optimally designed nanolayered metal-dielectric particles as probes for massively multiplexed and ultrasensitive molecular assays," Proc. Natl. Acad. Sci. **107**, 13620–13625 (2010).
60. L. Meng, R. Yu, M. Qiu, and F. J. García de Abajo, "Plasmonic Nano-Oven by Concatenation of Multishell Photothermal Enhancement," ACS Nano **11**, 7915–7924 (2017).
61. A. Moroz, "A recursive transfer-matrix solution for a dipole radiating inside and outside a stratified sphere," Annals Phys. **315**, 352–418 (2005).
62. N. Kongsuwan, A. Demetriadou, R. Chikkaraddy, F. Benz, V. A. Turek, U. F. Keyser, J. J. Baumberg, and O. Hess, "Suppressed Quenching and Strong-Coupling of Purcell-Enhanced Single-Molecule Emission in Plasmonic Nanocavities," ACS Photonics **5**, 186–191 (2018).
63. R. Faggiani, J. Yang, and P. Lalanne, "Quenching, Plasmonic, and Radiative Decays in Nanogap Emitting Devices," ACS Photonics **2**, 1739–1744 (2015).
64. N. Sakamoto, T. Onodera, T. Dezawa, Y. Shibata, and H. Oikawa, "Highly Enhanced Emission of Visible Light from Core-Dual-Shell-Type Hybridized Nanoparticles," Part. & Part. Syst. Charact. p. 1700258 (2017).
65. R. Kamakura, S. Murai, S. Ishii, T. Nagao, K. Fujita, and K. Tanaka, "Plasmonic-Photonic Hybrid Modes Excited on

Optical Materials EXPRESS

a Titanium Nitride Nanoparticle Array in the Visible Region," ACS Photonics **4**, 815–822 (2017).
66. Y. S. Kim, P. Leung, and T. F. George, "Classical decay rates for molecules in the presence of a spherical surface: A complete treatment," Surf. Sci. **195**, 1–14 (1988).
67. P. Bharadwaj, B. Deutsch, and L. Novotny, "Optical Antennas," Adv. Opt. Photonics **1**, 438 (2009).
68. C. F. Bohren and D. R. Huffman, *Absorption and Scattering of Light by Small Particles* (Wiley-VCH Verlag GmbH, Weinheim, Germany, 1998).
69. W. Zhu, R. Esteban, A. G. Borisov, J. J. Baumberg, P. Nordlander, H. J. Lezec, J. Aizpurua, and K. B. Crozier, "Quantum mechanical effects in plasmonic structures with subnanometre gaps," Nat. Commun. **7**, 11495 (2016).
70. G. Raschke, S. Brogl, A. S. Susha, A. L. Rogach, T. A. Klar, J. Feldmann, B. Fieres, N. Petkov, T. Bein, A. Nichtl, and K. Kürzinger, "Gold Nanoshells Improve Single Nanoparticle Molecular Sensors," Nano Lett. **4**, 1853–1857 (2004).
71. V. I. Zakomirnyi, I. L. Rasskazov, S. V. Karpov, and S. P. Polyutov, "New ideally absorbing Au plasmonic nanostructures for biomedical applications," J. Quant. Spectrosc. Radiat. Transf. **187**, 54–61 (2017).
72. C. G. Granqvist and O. Hunderi, "Optical absorption of ultrafine metal spheres with dielectric cores," Zeitschrift fur Physik B Condens. Matter Quanta **30**, 47–51 (1978).
73. B. N. Khlebtsov and N. G. Khlebtsov, "Biosensing potential of silica/gold nanoshells: Sensitivity of plasmon resonance to the local dielectric environment," J. Quant. Spectrosc. Radiat. Transf. **106**, 154–169 (2007).
74. P. B. Johnson and R. W. Christy, "Optical Constants of the Noble Metals," Phys. Rev. B **6**, 4370–4379 (1972).
75. U. Kreibig and M. Vollmer, *Optical Properties of Metal Clusters*, vol. 25 of *Springer Series in Materials Science* (Springer Berlin Heidelberg, Berlin, Heidelberg, 1995).
76. V. S. Gerasimov, A. E. Ershov, S. V. Karpov, A. P. Gavrilyuk, V. I. Zakomirnyi, I. L. Rasskazov, H. Ågren, and S. P. Polyutov, "Thermal effects in systems of colloidal plasmonic nanoparticles in high-intensity pulsed laser fields [Invited]," Opt. Mater. Express **7**, 555 (2017).
77. D. Zhou, D. Liu, W. Xu, X. Chen, Z. Yin, X. Bai, B. Dong, L. Xu, and H. Song, "Synergistic Upconversion Enhancement Induced by Multiple Physical Effects and an Angle-Dependent Anticounterfeit Application," Chem. Mater. **29**, 6799–6809 (2017).
78. D. Zhou, D. Liu, J. Jin, X. Chen, W. Xu, Z. Yin, G. Pan, D. Li, and H. Song, "Semiconductor plasmon-sensitized broadband upconversion and its enhancement effect on the power conversion efficiency of perovskite solar cells," J. Mater. Chem. A **5**, 16559–16567 (2017).
79. D. Zhou, D. Li, X. Zhou, W. Xu, X. Chen, D. Liu, Y. Zhu, and H. Song, "Semiconductor Plasmon Induced Up-Conversion Enhancement in mCu 2- x S@SiO 2 @Y 2 O 3 :Yb 3+ /Er 3+ Core-Shell Nanocomposites," ACS Appl. Mater. & Interfaces **9**, 35226–35233 (2017).
80. G. V. Naik, J. L. Schroeder, X. Ni, A. V. Kildishev, T. D. Sands, and A. Boltasseva, "Titanium nitride as a plasmonic material for visible and near-infrared wavelengths," Opt. Mater. Express **2**, 478 (2012).
81. G. V. Naik, V. M. Shalaev, and A. Boltasseva, "Alternative Plasmonic Materials: Beyond Gold and Silver," Adv. Mater. **25**, 3264–3294 (2013).
82. M. W. Knight, N. S. King, L. Liu, H. O. Everitt, P. Nordlander, and N. J. Halas, "Aluminum for Plasmonics," ACS Nano **8**, 834–840 (2014).
83. A. Lalisse, G. Tessier, J. Plain, and G. Baffou, "Quantifying the Efficiency of Plasmonic Materials for Near-Field Enhancement and Photothermal Conversion," The J. Phys. Chem. C **119**, 25518–25528 (2015).
84. J. R. Allardice and E. C. Le Ru, "Convergence of Mie theory series: criteria for far-field and near-field properties," Appl. Opt. **53**, 7224 (2014).